

Examining the role of flare-driven D-region electron density enhancement on Doppler Flash

Shibaji Chakraborty¹, Liying Qian², J. Michael Ruohoniemi¹, Joseph Baker¹, and Joseph McInerney²

¹Virginia Tech

²NCAR

November 21, 2022

Abstract

Trans-ionospheric high frequency (HF) signals experience a strong attenuation following a solar flare, commonly referred to as Short-Wave Fadeout (SWF). Although solar flare-driven HF absorption is a well-known impact of SWF, the occurrence of a frequency shift on radio wave signal traversing the lower ionosphere in the early stages of SWF, also known as “Doppler Flash”, is newly reported and not well understood. Some prior investigations have suggested two possible sources that might contribute to the manifestation of Doppler Flash: first, enhancements of plasma density in the D and lower E regions; second, the lowering of the reflection point in the F region. Observations and modeling evidence regarding the manifestation and evolution of Doppler Flash in the ionosphere are limited. This study seeks to advance our understanding of the initial impacts of solar flare-driven SWF. We use WACCM-X to estimate flare-driven enhanced ionization in D, E, and F-regions and a ray-tracing code (Pharlap) to simulate a 1-hop HF communication through the modified ionosphere. Once the ray traveling path has been identified, the model estimates the Doppler frequency shift along the ray path. Finally, the outputs are validated against observations of SWF made with SuperDARN HF radars. We find that changes in refractive index in the D and lower E regions due to plasma density enhancement are the primary cause of Doppler Flash.

Role of Flare-Driven Electron Density Change on Doppler Flash

S. Chakraborty (1), L. Qian (2), J. M. Ruohoniemi (1), J. B. H. Baker (1), J. M. McInerney (2)

(1) Virginia Tech, USA

(2) High Altitude Observatory, NCAR, USA



PRESENTED AT:



INTRODUCTION

- Trans-ionospheric high frequency (HF) signals experience a strong attenuation following a solar flare, commonly referred to as the Dellinger effect [Dellinger, 1937] or Short-Wave Fadeout (SWF).
- Although solar flare-driven HF absorption is a well-known space weather phenomenon [Fiori et al. 2018], the occurrence of a frequency shift on radio wave signal traversing the ionosphere in the early stage of SWF, also known as "Doppler Flash" [Chakraborty et al. 2018], is newly reported and less understood.
- Prior investigations have suggested two possible sources that might contribute to the manifestation of Doppler Flash:
 1. Change in refractive index due to the enhancement of plasma density in the D and lower E regions.
 2. Lowering of the ray reflection point in the F region.

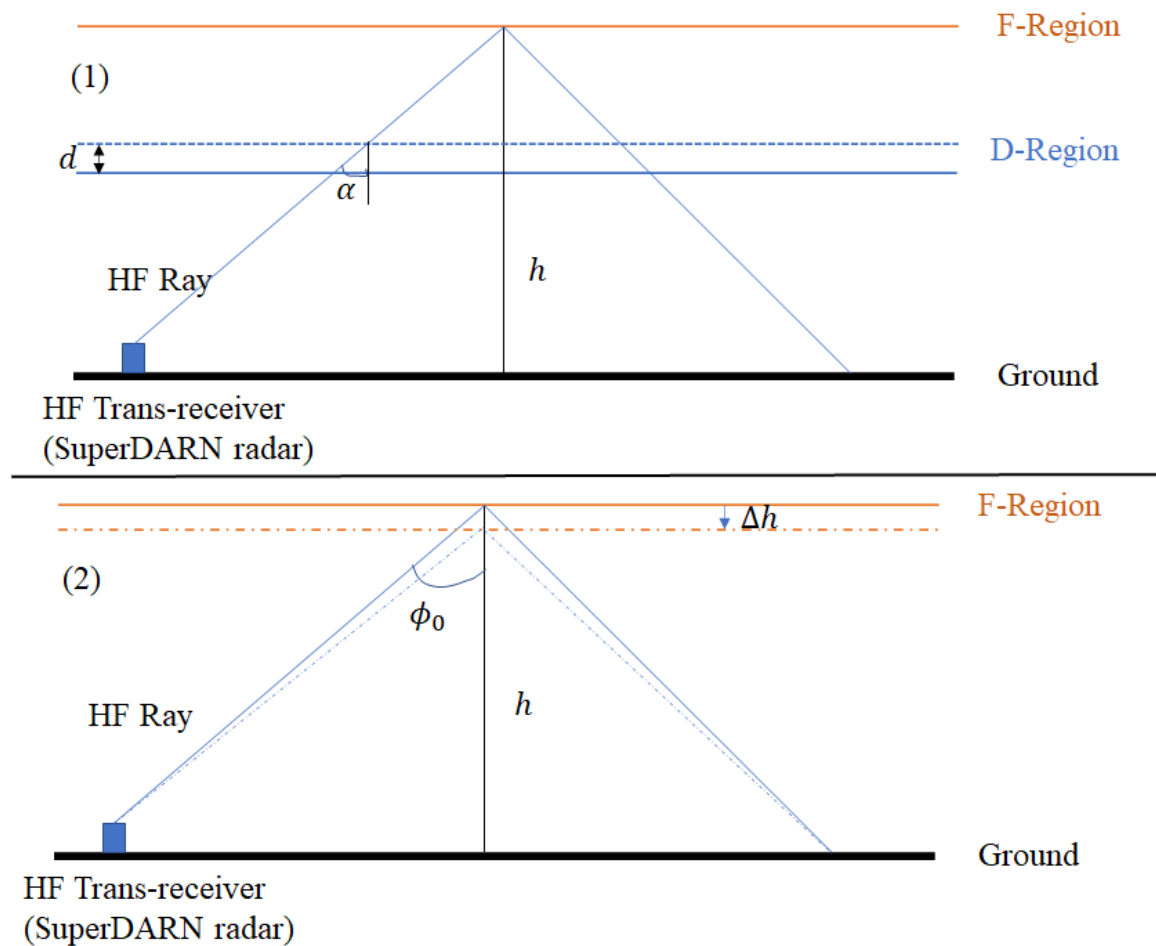


Figure 1: Illustration of two sources of Doppler flash (Adopted from Kikuchi et al. [1986]): (1) change in refractive index (due to change in electron density) below the reflecting height, (2) lowering the F-region reflecting height.

- This study seeks to advance our understanding of the initial impacts of solar flare-driven SWF using a first principle-based model.
- Model outputs are validated against observations from SuperDARN HF radars.

Questions:

1. Is the Doppler Flash primarily a D and lower E region phenomenon?
2. Does a solar flare impact the HF signal through the height change of the F region?

INSTRUMENT: SUPERDARN

Super Dual Auroral Radar Network (SuperDARN) is a network of HF radars, operating between 8 and 18 MHz, distributed worldwide. Each radar observes the line-of-sight (LoS) component of the $\vec{E} \times \vec{B}$ drift velocity of decameter-scale ionospheric plasma irregularities (Chisham et al., 2007; Greenwald et al., 1985; Nishitani et al., 2019).

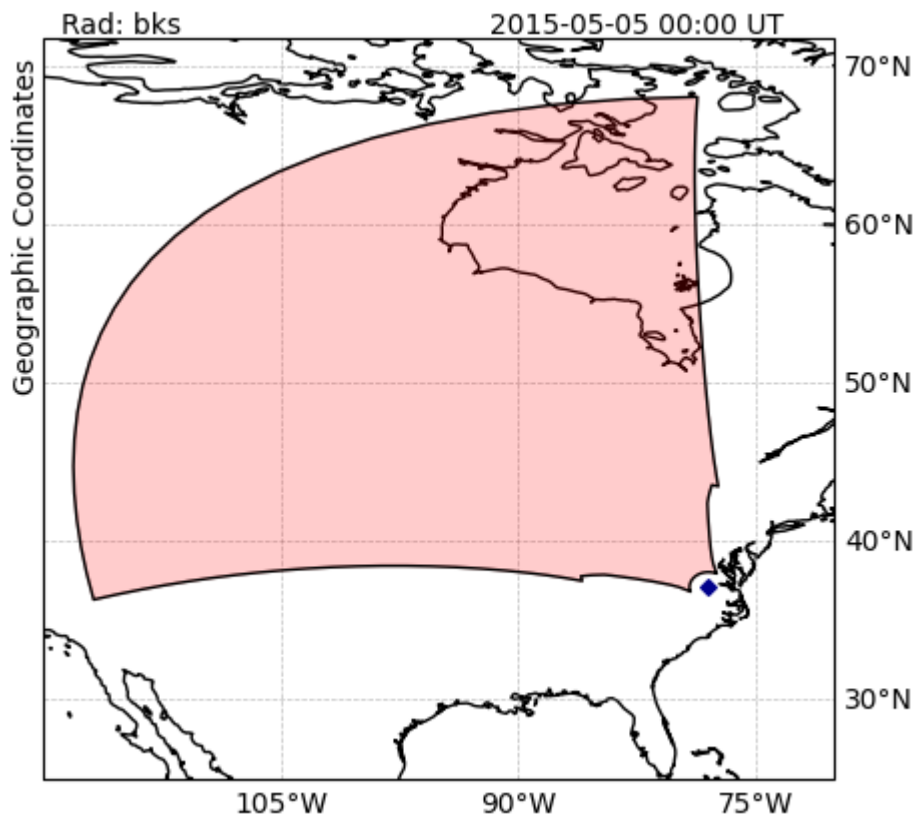


Figure 2: Location of the SuperDARN Blackstone radar and its corresponding fields-of-view (FoV).

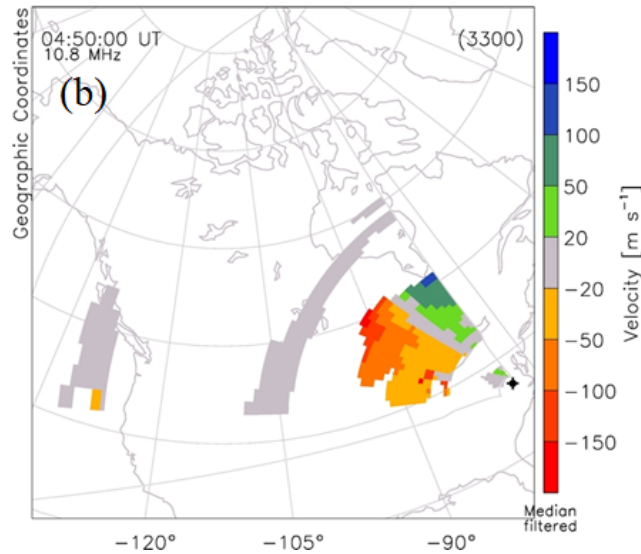
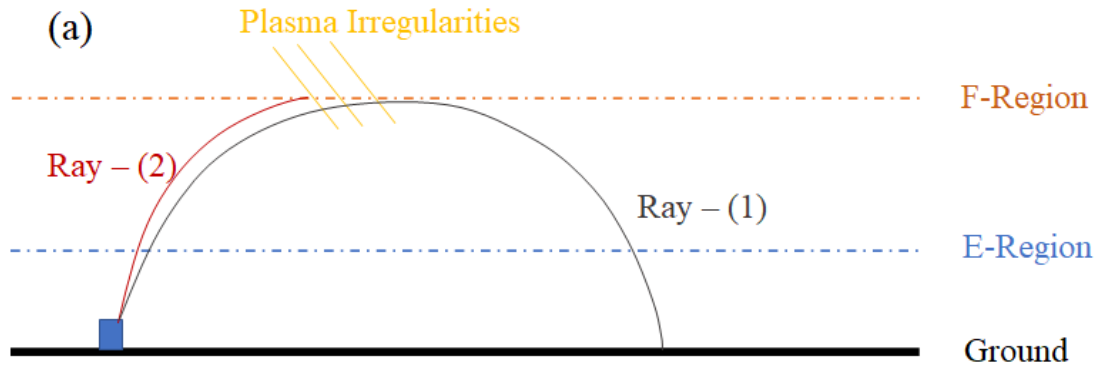


Figure 3: (a) Ray-paths for backscatter from the ground (Ray-1) and ionospheric irregularities (Ray-2). (b) An example FoV map of radar backscatter color-coded by Doppler velocity identifying regions of ground scatter (gray) and ionospheric scatter (colored).

- SuperDARN observations primarily consist of two types of backscatter; namely, ground scatter [Ray (1) of Figure 3a], and ionospheric scatter [Ray (2) of Figure 3a].
- Due to the high daytime vertical gradient in the refractive index, the rays bend toward the ground and are reflected from surface roughness and return to the radar following the same paths. This simulates a one-hop ground-to-ground communication link that passes through the D-region four times.
- Ionospheric scatter is the reflection of the transmitted signal from ionospheric plasma irregularities.
- Gray bands in Figure 3b presents low-velocity ground scatter and near range high velocity colored band represents ionospheric scatter.

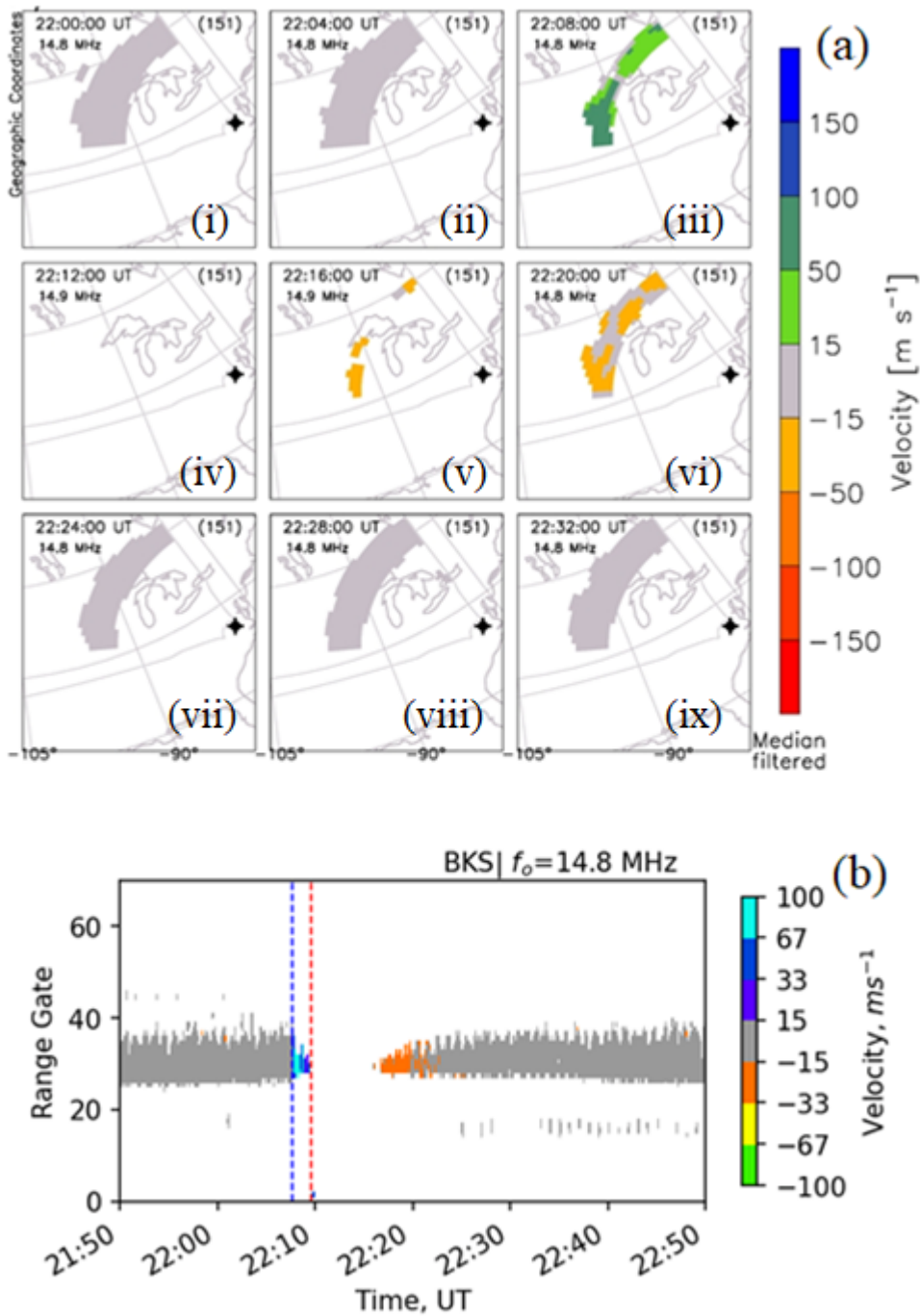


Figure 4: An SWF event seen by the Blackstone radar in response to a solar flare at 22:11 UT on 5 May 2015.

- Figure 4 shows a complete elimination of radar backscatter signal at 22:12 UT (panel a-iv), the HF absorption phase of SWF, while Figure 4b shows that the SWF phenomenon lasts on the order of tens of minutes and gradually restores back to normal (pre-SWF) condition with some negative shifts in Doppler velocity.
- The radio blackout event was preceded by a sudden enhancement of apparent backscatter Doppler velocity at 22:08 UT (refer to Figure 4(a-iii) and 4b), typically referred to as the "Doppler Flash" [Chakraborty et al., 2018].

MODELS: FISM, WACCM-X, AND HF DOPPLER MODEL

- We used three models, namely WACCM-X [H.-L. Liu et al., 2010; H.-L. Liu, Bardeen, et al., 2018], FISM [Chamberlin, 2008], and the Pharlap ray-tracing model [Cervera et al. 2014].
- The FISM and WACCM-X models estimate enhanced solar irradiance and ionospheric electron density following a solar flare.
- The Pharlap is used to geo-locate trans-ionospheric HF waves.
- Finally, we apply the Doppler theory described by Kikuchi [1986] to estimate Doppler shifts experienced by the traveling HF radio waves.

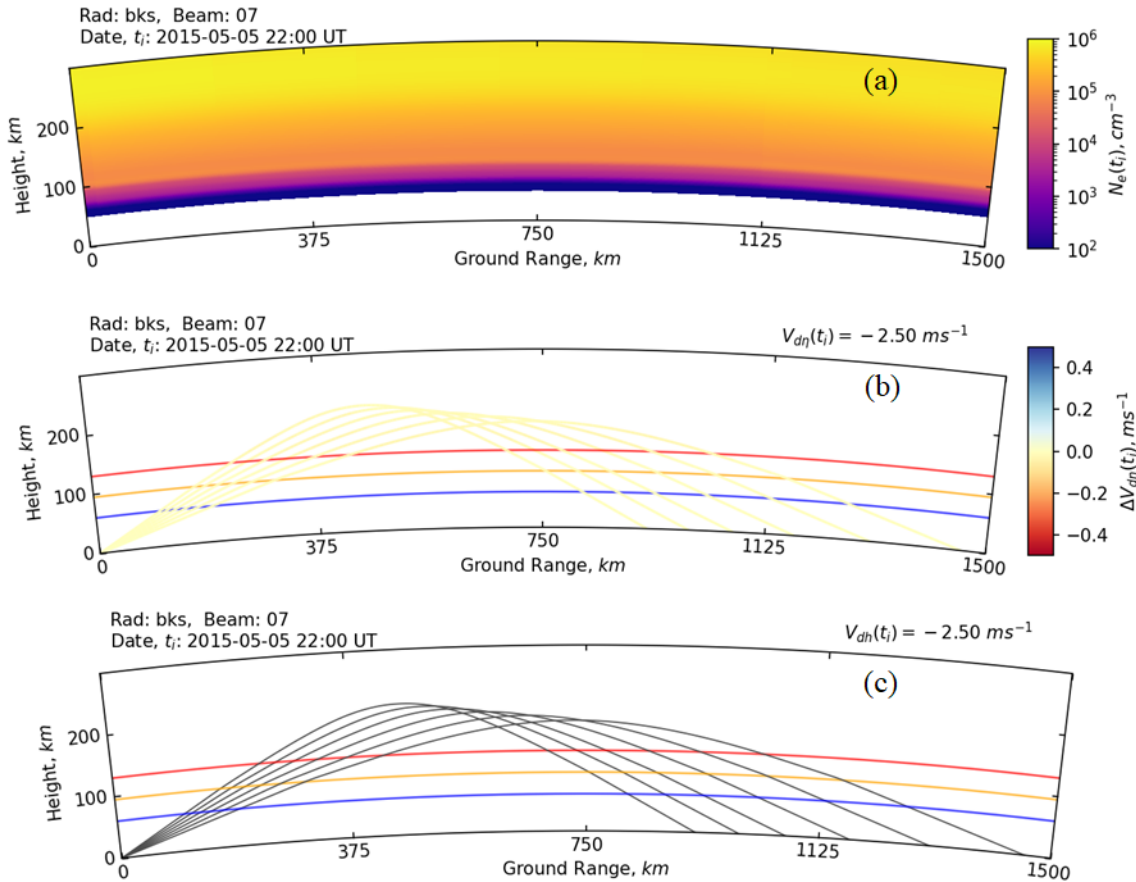


Figure 5: Ionospheric electron density and propagation condition along beam 7 of the SuperDARN Blackstone radar before a solar flare (5 May 2015, 22:00 UT): (a) electron density, (b) modeled Doppler velocity due to change in refractive index, and (c) modeled Doppler velocity due to lowering of the F region reflection point.

1. Electron density (in cm^{-3}) simulated by the WACCM-X model.
2. Modeled Doppler velocity along with the transmitted rays due to change in refractive index (in ms^{-1}).
3. Modeled Doppler velocity due to lowering the peak of the F-region reflection point (in ms^{-1}).
4. Horizontal blue, orange, and red lines in panels (b) and (c) represent approximate lower boundaries of D, E, and F regions, respectively.
5. Median Doppler velocity due to change in refractive index and lowering the F-region heights are provided in the top right corners of panels (b) and (c).

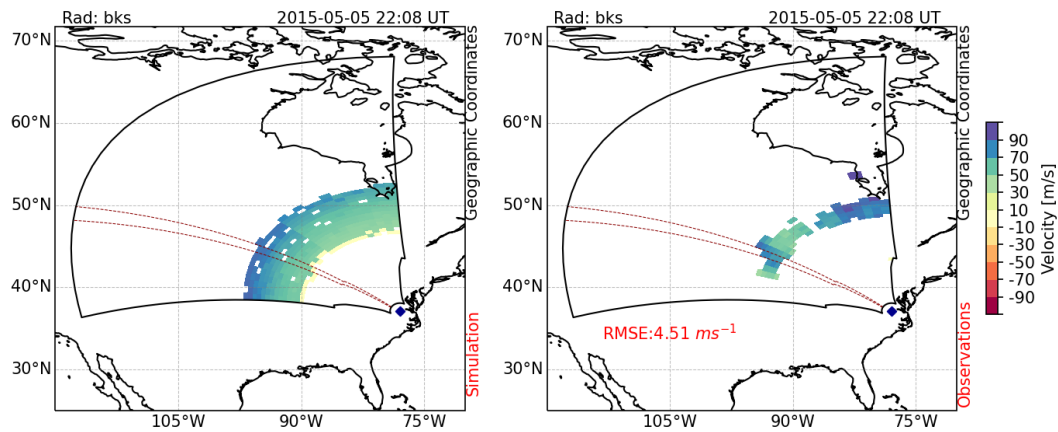


Figure 6: Data-model comparison for Blackstone SuperDARN radar at the peak of the Doppler flash (5 May 2015, 22:08 UT). Left and right panels show Doppler velocity estimated using the model and observation from the Blackstone radar. Doppler velocity is color-coded by the color-bar on the right. RMSE is provided in the right panel. The region enclosed by the red dashed lines represents beam 7 of the radar.

The model is able to replicate observations during the peak of the Doppler flash with an RMSE of $4.51 m s^{-1}$. In the next section, we only consider one beam (indicated by the red dashed line) to do a comprehensive data-model comparison. A movie is attached to this iPoster, see link below:

EVENT STUDY: 5 MAY 2015

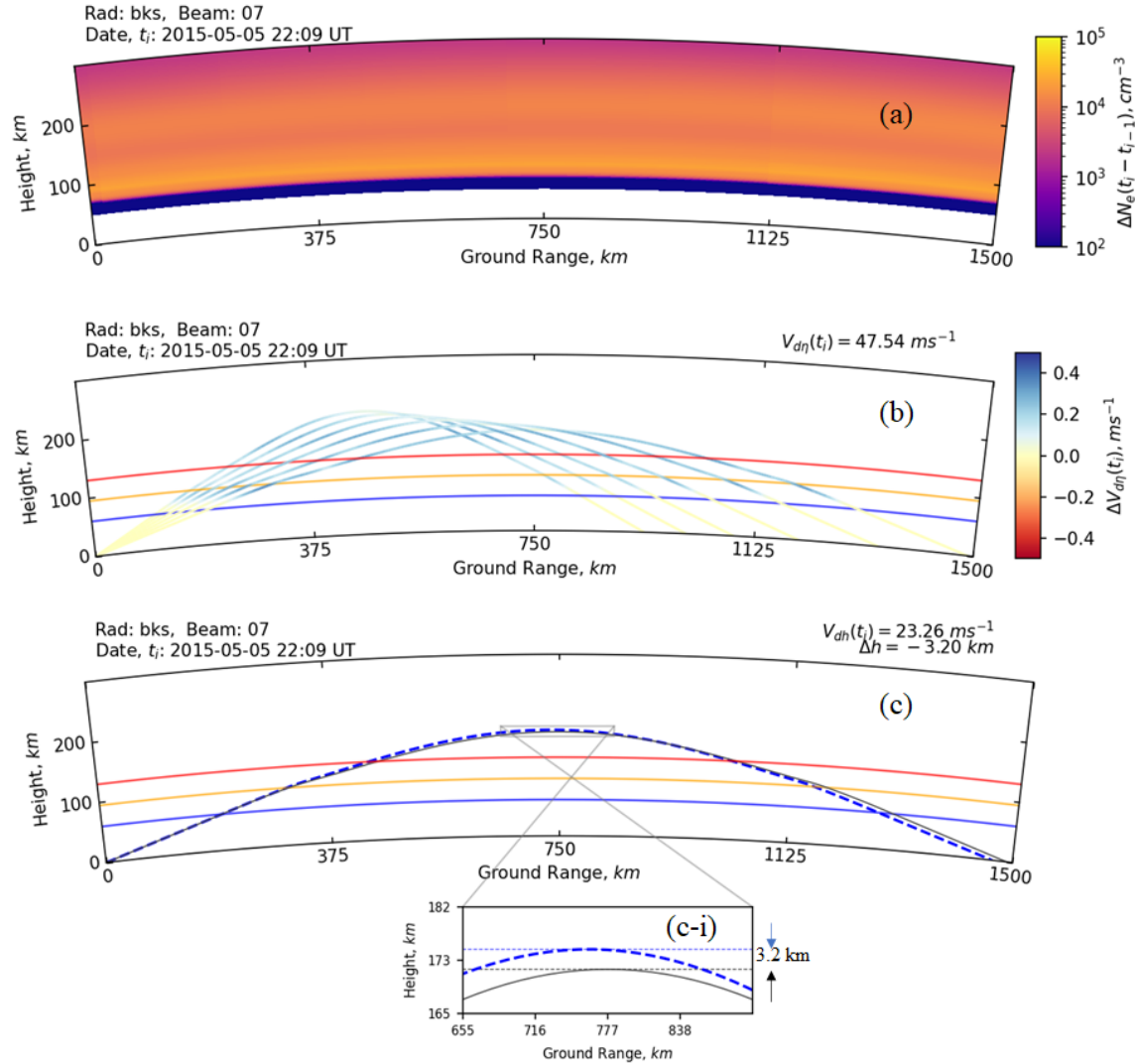


Figure 7: Change in ionospheric electron density and propagation condition along beam 7 of SuperDARN Blackstone radar during a solar flare on 5 May 2015, 22:09 UT: (a) differential electron density, (b) modeled Doppler velocity due to change in refractive index, (c) modeled Doppler velocity due to lowering of the F region reflection point, and (c-i) zoomed-in presents the zoomed-in version of the panel (c) to show the drop in the F region reflection point.

1. Top panel: differential electron density in (cm^{-3}), simulated by the WACCM-X model. The difference is taken from the electron density estimated from the previous timestep (t_{i-1}).
2. Middle panel: modeled Doppler velocity along with the transmitted rays due to change in refractive index (in ms^{-1}).
3. Bottom panel: modeled Doppler velocity due to lowering of the peak of the F-region reflection point (in ms^{-1}).
4. Panel (c-i) presents the zoomed-in version of panel (c) to show the drop in the F region reflection point. The dotted ray in the panel is the ray from the previous timestep (t_{i-1}) to show the change in the ray reflection point.
5. Horizontal blue, orange, and red lines in panels (b) and (c) represent approximate lower boundaries of D, E, and F regions, respectively. Median Doppler velocity due to change in refractive index, lowering the F-region heights, and change in reflection height are provided in the top right corners of panels (b) and (c), respectively.

Remark: The analysis suggests the relative contributions to the Doppler flash from changes in refractive index and lowering the F region reflection height are $\frac{2}{3}$ and $\frac{1}{3}$, respectively. The drop in reflection height is almost 3.2 km which is ~ 10 times bigger than the pre-flare condition (not shown here).

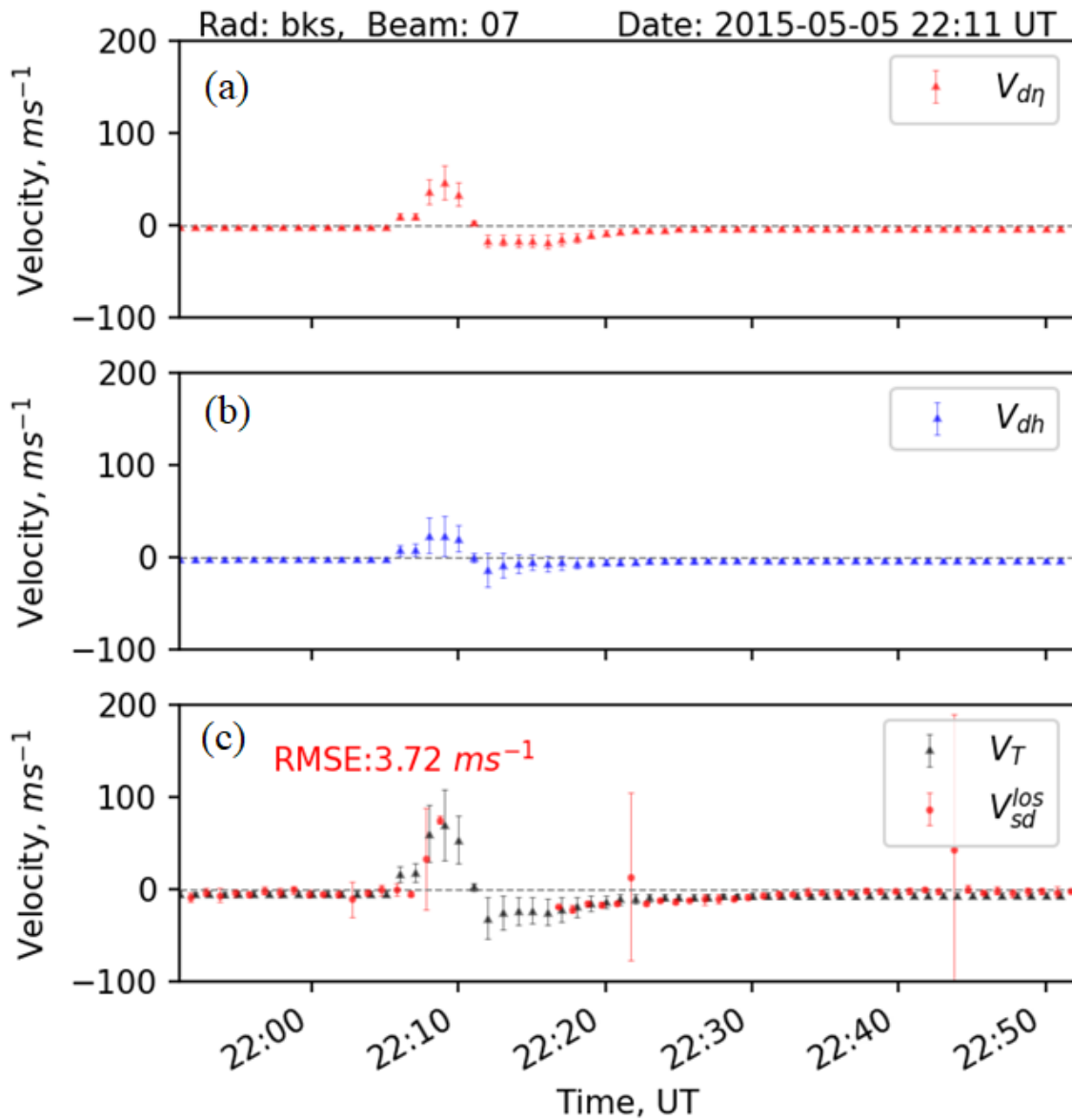


Figure 8: Time series plot showing data-model comparison along beam 7 (region enclosed by the red dashed lines in Figure 6) of SuperDARN Blackstone radar during a solar flare on 5 May 2015: (a) modeled Doppler velocity due to change in refractive index, (b) modeled Doppler velocity due to lowering of the F-region reflection point, and (c) total Doppler velocity estimated using the model. The red dots at the bottom panel is observations from SuperDARN Blackstone radar along beam 7.

1. Error bars in all panels present the range of Doppler velocity for different elevation angles along beam 7.
2. The comparison shows the total Doppler velocity estimated by the model along beam 7 of BKS radar replicates observations with an RMSE of 3.72 ms^{-1} .

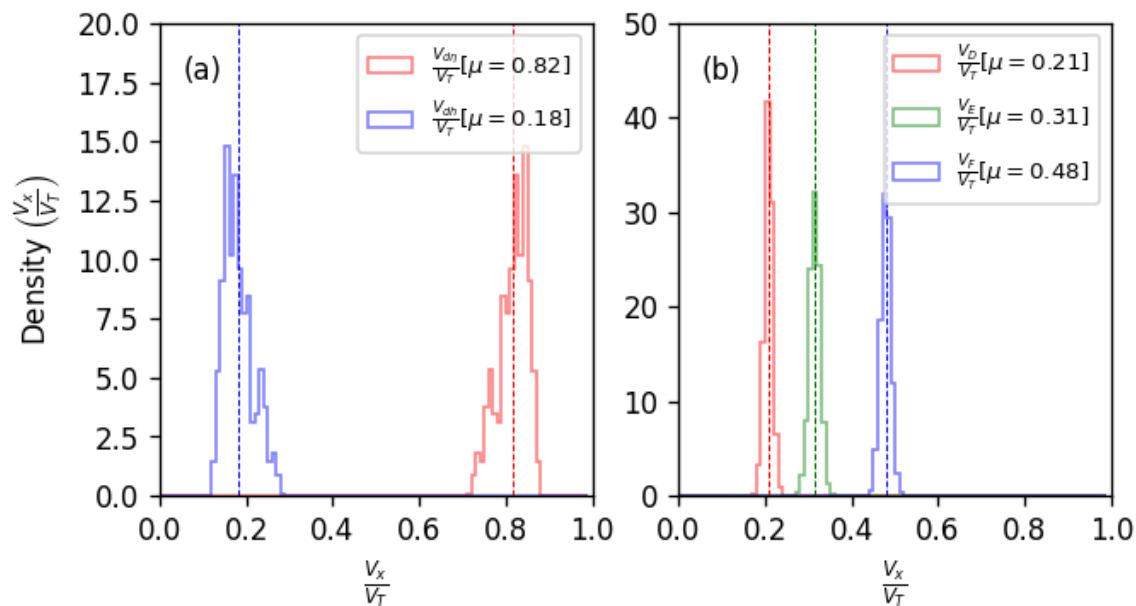


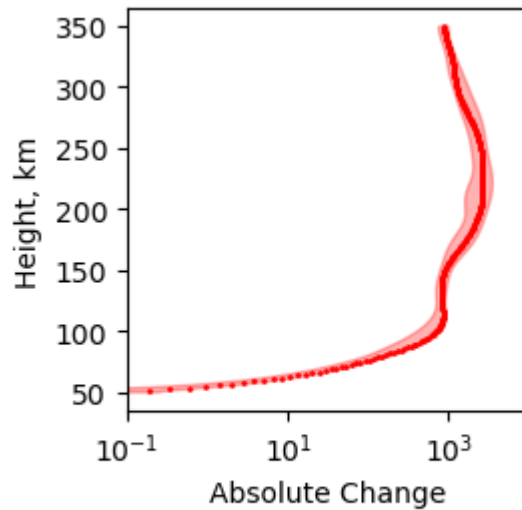
Figure 9: Histograms of (a) percentage Doppler velocity contributed by the change in refractive index (in red) and lowering the F-region reflection point (in blue), (b) percentage Doppler velocity contributed by D, E, and F regions in red, green, and blue, respectively. Mean μ for each population is provided in the legend.

The histograms are generated using simulation results for all beams of the BKS SuperDARN radar during the Doppler Flash at 22:07 - 22:09 UT on 5 May 2015.

DISCUSSION

Kikuchi et al. [1986] suggested solar flare driven Doppler flash contributed by the change in refractive index is predominantly a D and E region phenomenon and the geomagnetic storm is the major driver for lowering the F-region reflection point. We found:

1. The major contribution to the Doppler Flash is the F region electron density change (refer to Figure 10). Model results show the F region contributes ~48% of the total Doppler flash, among which ~18% is due to change in height and ~30% is due to a change in density.



$$\Delta N_e = N_e(t_i) - N_e(t - 1)$$

Figure 10: Height profile of change in electron density with time. N_e is calculated using the WACCM-X model.

Although, the percentage change of N_e in the D region is the highest, the absolute change of N_e is highest in the F region.

2. The downward movement of the F region is due to the enhanced electron density due to the photoionization caused by the enhanced EUVs during solar flare [Richards et al., 1988]. This downward movement of the F region may also be related to the weakening of the vertical ion drift in response to the solar flare [Qian et al., 2012].

CONCLUSION & FUTURE WORK

In this study, we have investigated the reasoning of Doppler flash observed by the SuperDARN HF radar following a solar flare. Specifically, we investigated the influence of the D, E, and F regions on Doppler flash.

By analyzing and comparing the modeled estimates against observations, we found:

1. Change in refractive index is the major driver of Doppler Flash (~82%) (see Figure 9).
2. Doppler flash contributed by the refractive index change is predominantly an E and F region phenomenon (see Figures 7 and 9).
3. Among D, E, and F regions, the F region is the major contributor to Doppler flash (~48% in total: ~18% is due to change in height and ~30% is due to a change in density) (see Figure 9).

Findings suggest the downward movement of the F region may also be related to the weakening of the vertical ion drift in response to the solar flare.

Future work: Our conclusions are based on the X2.7 class flare on 5 May 2015. Our future work will investigate other solar flares and perform a statistical study to find out whether these conclusions hold true to solar flare effects on Doppler flash in general.

AUTHOR INFORMATION

S. Chakraborty, Virginia Tech, USA

L. Qian, High Altitude Observatory, NCAR, USA

ABSTRACT

Trans-ionospheric high frequency (HF) signals experience a strong attenuation following a solar flare, commonly referred to as Short-Wave Fadeout (SWF). Although solar flare-driven HF absorption is a well-known impact of SWF, the occurrence of a frequency shift on radio wave signal traversing the lower ionosphere in the early stages of SWF, also known as "Doppler Flash", is newly reported and not well understood. Some prior investigations have suggested two possible sources that might contribute to the manifestation of Doppler Flash: first, enhancements of plasma density in the D and lower E regions; second, the lowering of the reflection point in the F region. Observations and modeling evidence regarding the manifestation and evolution of Doppler Flash in the ionosphere are limited. This study seeks to advance our understanding of the initial impacts of solar flare-driven SWF. We use WACCM-X to estimate flare-driven enhanced ionization in D, E, and F-regions and a ray-tracing code (Pharlap) to simulate a 1-hop HF communication through the modified ionosphere. Once the ray traveling path has been identified, the model estimates the Doppler frequency shift along the ray path. Finally, the outputs are validated against observations of SWF made with SuperDARN HF radars. We find that changes in the refractive index in the D and lower E regions due to plasma density enhancement are the primary cause of Doppler Flash.

REFERENCES

- Chakraborty, S., Ruohoniemi, J. M., Baker, J. B. H., & Nishitani, N. (2018). Characterization of short-wave fadeout seen in daytime SuperDARN ground scatter observations. *Radio Science*, 53, 472–484. <https://doi.org/10.1002/2017RS006488>
- Dellinger, J. (1937). Sudden disturbances of the ionosphere. *Proceedings of the Institute of Radio Engineers*, 25, 1253–1290.
- Kikuchi, T., Sugiuchi, T., Ishimine, M. H., & Shige-hisa, H. (1986). Solar-terrestrial disturbances of June-September 1982. IV. Ionospheric disturbances. 11. HF Doppler observations. *Journal of the Radio Research Laboratory*, 33(1), 239–255.
- Watanabe, D., & Nishitani, N. (2013). Study of ionospheric disturbances during solar flare events using the SuperDARN Hokkaido radar. *Advances in Polar Science*, 24(1), 12–18.
- Fiori, R. A. D., Koustov, A. V., Chakraborty, S., Ruohoniemi, J. M., Danskin, D. W., Boteler, D. H., & Shepherd, S. G. (2018). Examining the Potential of the Super Dual Auroral Radar Network for Monitoring the Space Weather Impact of Solar X-Ray Flares. *Space Weather*, 16, 1348–1362. <https://doi.org/10.1029/2018SW001905>
- Chisham, G., Lester, M., Milan, S., Freeman, M., Bristow, W., Grocott, A., et al. (2007). A decade of the Super Dual Auroral Radar Network (SuperDARN): Scientific achievements, new techniques and future directions. *Surveys in Geophysics*, 28, 33–109. <https://doi.org/10.1007/s10712-007-9017-8>
- Greenwald, R. A., Baker, K. B., Hutchins, R. A., & Hanuise, C. (1985). An HF phased-array radar for studying small-scale Structure in the high-latitude ionosphere. *Radio Science*, 20(1), 63–79. <https://doi.org/10.1029/RS020i001p00063>
- Nishitani, N., Ruohoniemi, J.M., Lester, M. et al. Review of the accomplishments of mid-latitude Super Dual Auroral Radar Network (SuperDARN) HF radars. *Prog Earth Planet Sci* 6, 27 (2019). <https://doi.org/10.1186/s40645-019-0270-5>
- Liu, H.-L. et al. (2010), Thermosphere extension of the Whole Atmosphere Community Climate Model, *J. Geophys. Res.*, 115, A12302, doi:10.1029/2010JA015586.
- Liu, H.-L., Bardeen, C. G., Foster, B. T., Lauritzen, P., Liu, J., Lu, G., et al. (2018). Development and validation of the whole atmosphere community climate model with thermosphere and ionosphere extension (WACCM-X v. 2.0). *Journal of Advances in Modeling Earth Systems*, 10(2), 381–402. <https://doi.org/10.1002/2017MS001232>.
- Liu, J., Liu, H., Wang, W., Burns, A. G., Wu, Q., Gan, Q., et al. (2018). First results from the ionospheric extension of WACCM-X during the deep solar minimum year of 2008. *Journal of Geophysical Research: Space Physics*, 123(2), 1534–1553. <https://doi.org/10.1002/2017JA025010>.
- Chamberlin, P. C., Woods, T. N., and Eparvier, F. G. (2008), Flare Irradiance Spectral Model (FISM): Flare component algorithms and results, *Space Weather*, 6, S05001, doi:10.1029/2007SW000372.
- Cervera, M. A., and Harris, T. J. (2014), Modeling ionospheric disturbance features in quasi-vertically incident ionograms using 3-D magnetoionic ray tracing and atmospheric gravity waves, *J. Geophys. Res. Space Physics*, 119, 431–440, doi:10.1002/2013JA019247
- Richards, P. G., and Torr, D. G. (1988), Ratios of photoelectron to EUV ionization rates for aeronomic studies, *J. Geophys. Res.*, 93(A5), 4060–4066, doi:10.1029/JA093iA05p04060.
- Qian, L., Burns, A. G., Solomon, S. C., and Chamberlin, P. C. (2012), Solar flare impacts on ionospheric electro-dynamics, *Geophys. Res. Lett.*, 39, L06101, doi:10.1029/2012GL051102.